CERN-PPE/90-184
11 December 1990



EUROPEAN ORGANIZATION FOR NUCLEAR RESEARCH

# Measurement of the Antiproton-Stopping Power of Gold - The Barkas Effect

R. Medenwaldt, S. P. Møller, E. Uggerhøj, and T. Worm

*Institute for Synchrotron Radiation, Aarhus University*
*Ny Munkegade, DK-8000 Aarhus C, Denmark*

P. Hvelplund and H. Knudsen

*Institute of Physics, University of Aarhus*
*DK-8000 Aarhus C, Denmark*

K. Elsener

*CERN, CH-1211 Geneve 23, Switzerland*

E. Morenzoni

*Paul Scherrer Institute, CH-5232 Villigen PSI, Switzerland*

**Abstract**

The stopping power of gold has been measured for antiprotons in the energy range 0.2-3 MeV using a novel Time-Of-Flight technique. The antiproton-stopping power is found to be less than half the equivalent proton stopping power near the electronic stopping power maximum. In the high-energy limit the two stopping powers merge.

(submitted to Phys. Letters A)

The slowing down of charged particles in matter is described by the energy loss per unit length, the stopping power. The collisions between the projectile and the target can be divided into inelastic collisions, usually referred to as electronic, where target atoms are excited or ionized, and elastic collisions, referred to as nuclear, where the whole target atom recoils. The nuclear stopping only contributes significantly at very low projectile velocities and can be neglected in the present context. The electronic stopping power has a maximum around the typical target electron velocity. For lower projectile velocities, the stopping power is velocity proportional and above the maximum, the stopping power decreases roughly inversely proportional to the projectile energy.

The stopping power has been extensively studied since the berginning of the century, both theoretically and experimentally, and in the region of very fast projectiles of low charge, the interaction is reasonably well understood. Around and below the electronic stopping-power maximum for protons measurements are not well reproduced by theoretical estimates. For negatively charged particles no direct measurements are available in this region[1,2] and even the qualitative behavior of the stopping power is unknown.

The basic stopping-power formula in the high-energy limit is the Bethe formula[3], which is derived in the first Born approximation. Hence the stopping power is proportional to the square of the projectile charge, $Z_1^2$. A $Z_1^3$ (Barkas) correction to the Bethe formula for the harmonic oscillator was first calculated by Ashley, Ritchie and Brandt[4] and by Jackson and McCarthy[5] for distant collisions only. The dividing impact parameter between close and distant collisions is of the order of the radius of the harmonic oscillator. The effect is related to the polarization of the medium induced by the projectile. This explains qualitatively why negatively charged particles have a lower stopping power than positive. Later Lindhard[6] argued, that the close collisions contribute to the Barkas effect with an equally important amount. It was also shown, that the $Z_1^4$ correction (the Bloch term) is significant. Recently, a rigorous calculation of the stopping

power up to third order in $Z_1$ for the harmonic oscillator has appeared[7], showing significant contributions to the Barkas term for *all* impact parameters. This calculation covers a wide region around the stopping-power maximum. In the velocity-proportional stopping region below the maximum, Sørensen[8] calculated an antiproton-stopping power of heavy elements of about half the proton value. A calculation of the Barkas term for energy loss in an electron gas in the high-energy region has also appeared recently[9].

Deviations from a $Z_1^2$ scaling of the stopping power was first signalled from observed range differences between pions of positive and negative charge[10]. These departures were later also investigated by comparing measured stopping powers for protons, alpha particles[11] and lithium nuclei[12]. For reviews of the experimental and theoretical situation, see Refs. 13,14 and 15.

Recently, a high-quality antiproton beam from LEAR at the CERN accelerator facility was used to accurately measure the Barkas term for silicon by comparisons of stopping powers for protons and antiprotons[16,17]. The method developed was limited to silicon, since the energy loss was inferred from the energy deposited in an active silicon detector. Furthermore, the method can not easily be extended to energies below 200 keV. The present work describes a new method capable of measuring the stopping power directly of most elements taking into account the special properties (see below) of a degraded low-energy antiproton beam.

The experiment used a 5.9-MeV antiproton beam from LEAR. The beam exits the LEAR vacuum system through a 100-$\mu$m beryllium window and enters the experimental-vacuum chamber through a 20-$\mu$m mylar foil as shown in fig. 1. Here the beam is degraded to lower energies by aluminium foils. Since both the incident and exit energies are required, we measure the Time-Of-Flight (TOF) of the particles from the 100-$\mu$m thick start scintillator to the target foil and from the foil to the 1-mm thick stop scintillator. The data are accumulated on an event-by-event basis using a CAMAC system connected to a PC. The timing signal from the target foil is obtained from the emitted secondary electrons. These electrons are accelerated from the foil, reflected by an

electrical mirror and further accelerated towards a detecting channel plate (fig. 1). The time resolution obtained is 2.7 ns (FWHM), which in the present setup corresponds to an energy resolution of 27 keV (FWHM) at 500 keV. The system is calibrated by standard delays and by varying the length of the flight paths. The efficiency of the system is rather low, owing to the low efficiency of the secondary electron detection (<10 %) and in particular because of the large multiple scattering of the antiprotons when degrading to energies below 1 MeV. The target foils used were 5, 2 and 1 $\mu$m gold foils.

For incident energies above 1 MeV, the beam is practically monoenergetic, but degradation to lower energies leads to a large energy spread. In fig. 2 the incident and exit TOF distribution is shown in the case of a 1 $\mu$m gold target foil and a 72-$\mu$m aluminium-degrader foil. It is seen that incident energies between 200 and 700 keV are covered by one degrader. "Monoenergetic" beams can then be selected in the analysis. The stopping power is determined as $dE/dx = \Delta E/\Delta x = (E_1 - E_2)/\Delta x$ at the energy $E_1 - \Delta E/2$, where $E_1$ is the incident energy, $E_2$ is the exit energy and $\Delta x$ the target thickness.

Fig. 3 shows the measured antiproton stopping power for the three different foils used. The errorbars are derived from an estimated 0.2 nsec. uncertainty in the determination of the centroid of the TOF distribution and a 5% uncertainty in the thickness of the foils used. This gives rise to a larger uncertainty at high energy owing to the small TOF and the small energy loss, as is also reflected from the scatter in the points. We observe, that results from different foils agree in the overlap regions.

The proton-stopping powers shown are from Refs. 18 (open circles) and 19 (full-drawn curve). The antiproton measurements merge with the shown proton-stopping powers at high energy, where it is known, that the Barkas effect is small[12]. Between 1.6 and 2.6 MeV/amu, stopping powers of p, $He^{++}$ and $Li^{3+}$ measured for a Au target by Andersen et al.[12] made it possible for these authors to deduce the $Z_1^3$ and $Z_1^4$ terms. Using these results, we have calculated the corresponding stopping power for antiprotons, as

shown in fig. 3 (open triangles). These results agree well with the present data.

At low energy the antiproton stopping power is more than a factor of two lower than for protons. Furthermore, the stopping power is constant within the experimental uncertainty and no characteristic maximum is observed for antiprotons as for protons.

We shall not here attempt a discussion of all the theoretical models available, but note that the present data allows comparisons with e.g. the harmonic-oscillator and electron-gas models from Refs. 7 and 9, respectively. The data can also be related to results in the velocity-proportional stopping region, i.e. below the stopping maximum. In this region Sørensen calculated an antiproton stopping power about half that of protons. This result nicely merges with the present measurements. In refs. 19 and 20, the stopping power of gold for protons was calculated including the Bethe, Barkas and Bloch terms using a local density approximation for the harmonic oscillator. The results compare very well with proton measurements[19]. Their approximations are only valid up to 300 keV, but the results converted to antiprotons (dashed curve) seem to overestimate our antiproton stopping power measurements between 200 and 300 keV. The present antiproton measurements are also connected to previous measurements of other atomic collision phenomena for negatively charged particles, e.g. inner-shell ionization[13, 21, 22, 23].

The first measurements of the Barkas effect with the new TOF method described here will be extended to other targets, to study the $Z_2$ dependence of the Barkas-term. Also measurements at lower energies seem possible. Finally it should be mentioned that the method used in the present experiment will allow the energy-loss straggling for antiprotons to be determined for the first time. The relative contribution from the close collisions to the straggling is larger than than to the stopping power, and hence straggling results together with stopping power results will probe the contributions from the close and distant collisions separately.

**References**

[1]W. Wilhelm, H. Daniel, and F. J. Hartmann, Phys. Lett. B **98**, 33 (1981).

[2]F. Kottmann, Proc. II Int. Symp. on Muon and Pion Interactions with Matter (Dubna, 1987).

[3]H.A.Bethe, Ann. Phys. (Leipzig) **5**, 325 (1930); U. Fano, Ann. Rev. Nucl. Sci. **13**,1 (1963).

[4]J. C. Ashley, R. H. Ritchie, and W. Brandt, Phys. Rev. B **5**, 2393 (1972); Phys. Rev. A **8**, 2402 (1973).

[5]J. D. Jackson and R. L. McCarthy, Phys. Rev. B **6**, 4131 (1972).

[6]J. Lindhard, Nucl. Instrum. Methods **132**, 1 (1976).

[7]H. H. Mikkelsen and P. Sigmund, Phys. Rev. A **40**, 101 (1989).

[8]A. H. Sørensen, Nucl. Instrum. Methods B **48**, 10 (1989).

[9]H. Esbensen and P. Sigmund, Ann. Phys. **201**, 152 (1990).

[10]W. H. Barkas, W. Birnbaum, and F. M. Smith, Phys. Rev. **101**, 778 (1956).

[11]H. H. Andersen, H. Simonsen, and H. Sørensen, Nucl. Phys. A **125**, 171 (1969).

[12]H. H. Andersen, J. F. Bak, H. Knudsen, and B. R. Nielsen, Phys. Rev. A **16**, 1929 (1977).

[13]G. Basbas, Nucl. Instrum. Methods B **4**, 227 (1984).

[14]H. H. Andersen, in *Semiclassical Descriptions of Atomic and Nuclear Collisions*, edited by J. Bang et al. (Elsevier, New York, 1985), p. 409.

[15]H. Bichsel, Phys. Rev. A **41**, 3642 (1990).

[16]L. H. Andersen, P. Hvelplund, H. Knudsen, S. P. Møller, J. O. P. Pedersen, E. Uggerhøj, K. ELsener, and E. Morenzoni, Phys. Rev. Lett. **62**, 1731 (1989).

[17]R. Medenwaldt, S. P. Møller, E. Uggerhøj, T. Worm, P. Hvelplund, H. Knudsen, K. Elsener, and E. Morenzoni, submitted to Nucl. Instrum. Methods B.

[18]H. H. Andersen and B. R. Nielsen, Nucl. Instrum. Methods **191**, 475 (1981).

[19]D. Semrad, Ch. Eppacher and R. Tober, Nucl. Instrum. Methods B **48**, 79 (1990).

[20]D. Semrad, private communication.

[21]L. H. Andersen, P. Hvelplund, H. Knudsen, S. P. Møller, J. O. P. Pedersen, S. Tang-Petersen, E. Uggerhøj, K. Elsener, and E. Morenzoni, Phys. Rev. A **41**, 6536 (1990).

[22]R. Medenwaldt, S. P. Møller, E. Uggerhøj, T. Worm, P. Hvelplund, H. Knudsen, K. Elsener, and E. Morenzoni, to be published.

[23]E. Morenzoni, invited talk at X90, preprint PSI PR-90-22 (1990), to be published in the proceedings.

**Figure Captions**

Fig. 1 Schematic drawing of the experimental setup. The numbers refer to: 1 Beamline vacuum chamber; 2 Start scintillator; 3 Target foil; 4 and 5 Electrical mirror; 6 Channelplate detector, 7 Stop scintillator.

Fig. 2 Scatter plot of the incident and exit antiproton-flight times. The projections are also shown (scales converted to antiproton energy).

Fig. 3 Measured antiproton-stopping power in different gold foils (filled circles, squares and triangles) compared to proton data[18,19] (open circles and full-drawn curve). The open triangles are antiproton-stopping powers deduced from ion measurements[12,18]. The dashed curve is the antiproton-stopping power predicted by the model in refs. 19 and 20.

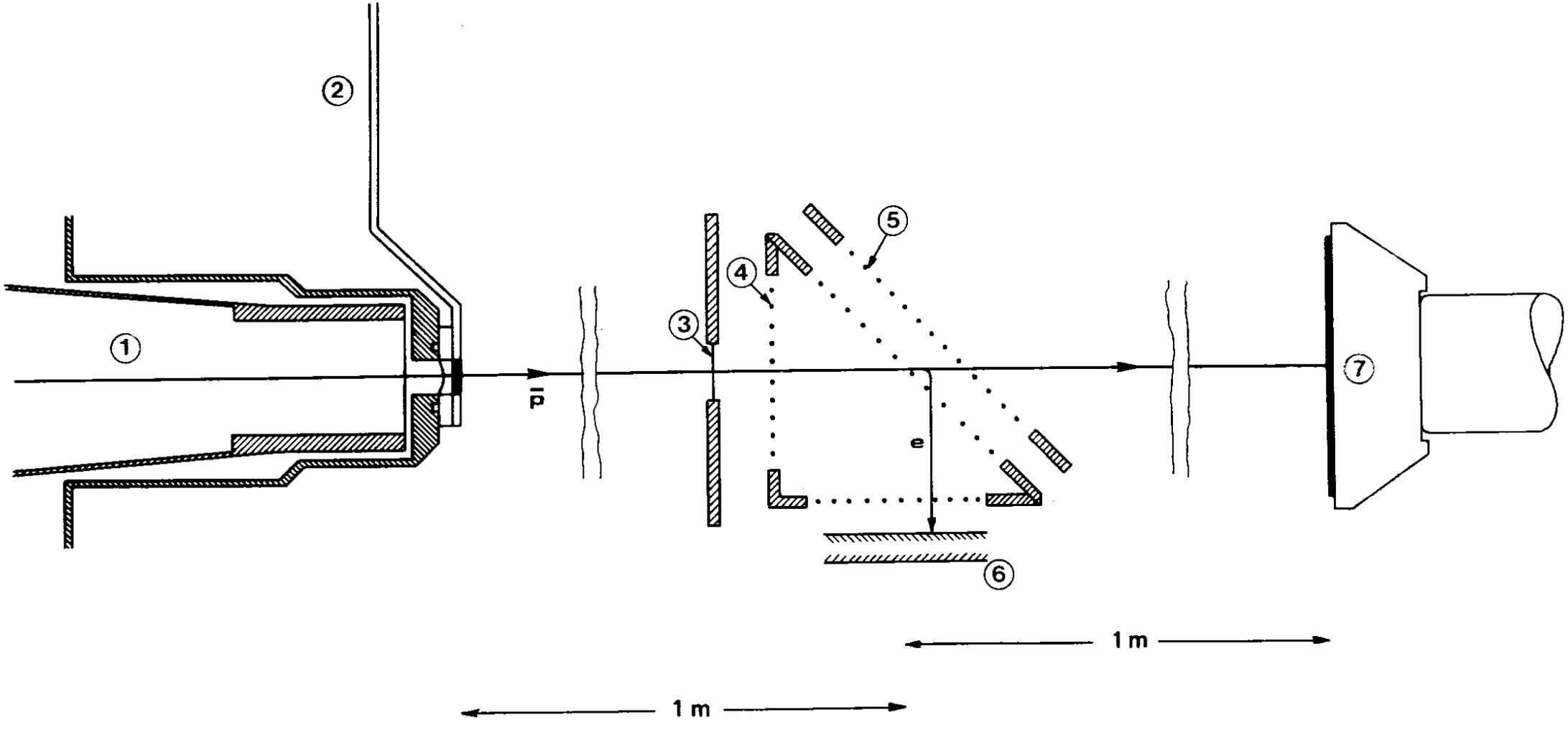


Fig. 1

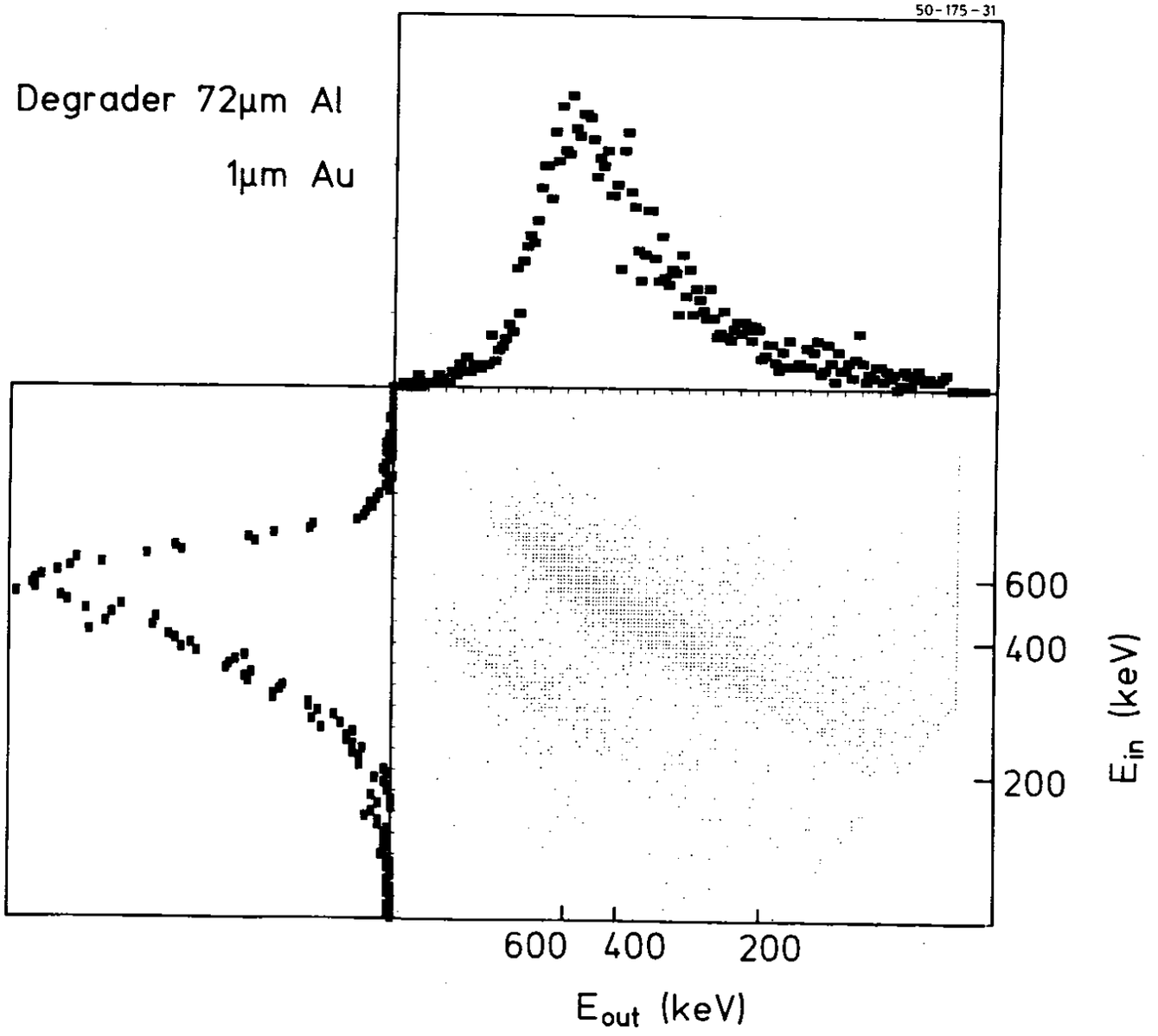
50-175-31
Degrader 72µm Al
1µm Au
600
400
200
$E_{in}$ (keV)
600 400 200
$E_{out}$ (keV)

Fig. 2

Imprimé au CERN. Prix : 0.35 Fr.

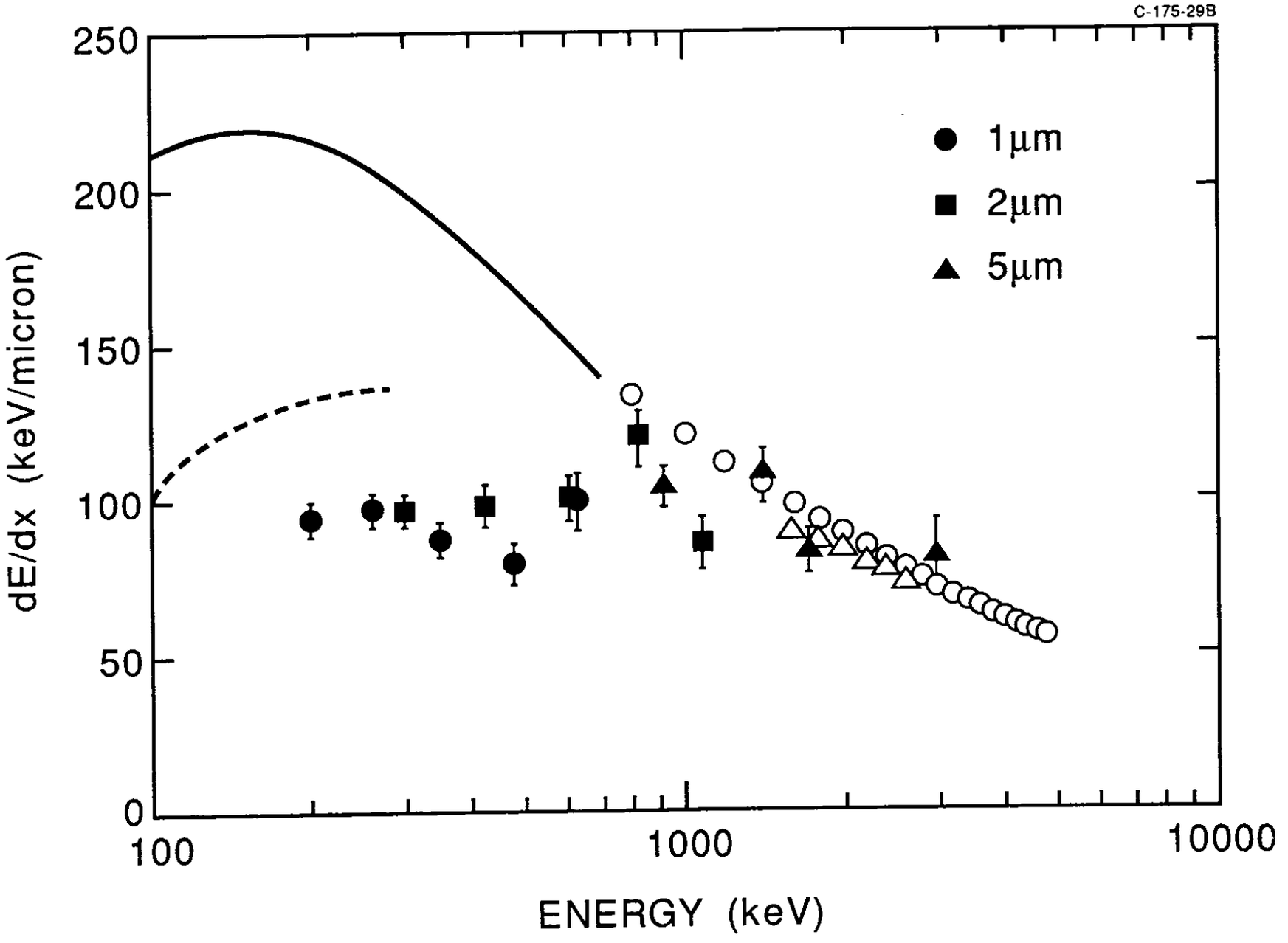


Fig. 3